Increased Efficiency of Dye-Sensitized Solar Cells by Incorporation of a π Spacer in Donor-Acceptor Zinc Porphyrins Bearing Cyanoacrylic Acid as an Anchoring Group

Stylianos Panagiotakis, Emmanouil Giannoudis, Asterios Charisiadis, Raphaella Paravatou, Maria-eleni Lazaridi, Maria Kandyli, Kalliopi Ladomenou, Panagiotis A Angaridis, Hélène C Bertrand, Ganesh D Sharma, et al.

Increased Efficiency of Dye-Sensitized Solar Cells by Incorporation of a π Spacer in Donor–Acceptor Zinc Porphyrins Bearing Cyanoacrylic Acid as an Anchoring Group

Stylianos Panagiotakis,[a][‡] Emmanouil Giannoudis,[a][‡] Asterios Charisiadis,[a] Raphaella Paravatou,[a] Maria-Eleni Lazaridi,[a] Maria Kandyli,[a] Kalliopi Ladomenou,[a] Panagiotis A. Angaridis,[b] Hélène C. Bertrand,*[c] Ganesh D. Sharma,*[d] and Athanassios G. Coutsolelos*[a]

Abstract: Two novel porphyrins, ZnP(SP)CNCOOH and ZnPCNCOOH, bearing cyanoacrylic acid as an anchoring group were synthesized. Porphyrin ZnP(SP)CNCOOH contains a π-conjugated spacer (SP) for improved electronic communication between the dye and the TiO_2 electrode. The spacer bears polyethylene glycol chains to prevent dye aggregation and to enhance solubility of the dye. Electrochemical measurements and theoretical calculations suggest that both porphyrins are promising sensitizers for dye-sensitized solar cells (DSSCs), as their molecular orbital energy levels favor electron injection and dye regeneration. Solar cells sensitized by ZnP(SP)CNCOOH and ZnPCNCOOH show power conversion efficiencies of 7.61 and 5.02 %, respectively. Photovoltaic measurements (*J*–*V* curves and incident photon to current conversion efficiency spectra) show that higher short-circuit current (J_{sc}) and open-circuit voltage (V_{oc}) values are reached for the solar cell based on ZnP(SP)CNCOOH. This can be mainly ascribed to suppressed charge recombination, as indicated by their electrochemical impedance spectra.

Introduction

The constantly growing consumption of global energy along with the depletion of fossil fuels have prompted scientists to explore clean and renewable energy sources. Among the various technologies that have been reported, photovoltaic devices and dye-sensitized solar cells (DSSCs), in particular, have drawn great attention as promising candidates for the utilization of solar energy leading to a sustainable society worldwide.[1] Since the first report of DSSCs,[2] numerous inorganic and organic compounds have been studied as sensitizers.[3] In photosynthetic organisms, solar irradiation is collected by chlorophylls and is consequently converted into chemical energy. Intrigued by that, a wide portion of chemists have studied artificial photosynthetic schemes based on porphyrins, which are the synthetic analogues of chlorophyll.[4] What is more, porphyrins have been proven to be ideal candidates for countless applications, as they possess several needed properties, such as strong absorption, great stability, tunable redox potentials, and easy modification and metal-ion insertion.[5]

During the last decades, porphyrin derivatives have been extensively studied in DSSCs,[6] and the best results have been achieved upon using push–pull-type porphyrins as sensitizers.[7] Up to date, the most efficient push–pull porphyrin-based photosensitizer was reported by Grätzel and co-workers, and it reached an efficiency of approximately 13 %.[8] Despite the fact that such push–pull sensitizers are highly efficient, their synthesis normally requires multistep routes with low overall yields, thus limiting their use in large-scale applications.[9] On the contrary, the synthesis of tetraarylporphyrins by condensation of pyrrole with an aldehyde requires fewer synthetic steps, and higher yields are achieved.[10]

A suitable anchoring group at the periphery of the macrocycle is necessary for the successful attachment of the sensitizer onto the semiconductor (i.e., TiO_2) surface. Porphyrins that contain carboxylic or cyanoacrylic acid as anchoring groups are

[a] *Department of Chemistry, University of Crete, Laboratory of Bioinorganic Chemistry,*
Voutes Campus, 70013 Heraklion, Crete, Greece
E-mail: coutsole@chemistry.uoc.gr
http://www.chemistry.uoc.gr/coutsolelos/
[b] *Department of Chemistry, Aristotle University of Thessaloniki, 54124 Thessaloniki, Greece*
http://www.chem.auth.gr/index.php
[c] *Laboratoire des Biomolécules - UMR7203, Département de Chimie de l'ENS,*
24 rue Lhomond et Campus Jussieu – Tour 23-33-5ème étage – 4 place Jussieu, 75005 Paris, France
E-mail: helene.bertrand@ens.fr
http://www.labos.upmc.fr/lbm/
[d] *Molecular Electronics and Optoelectronic Research Laboratory, Department of Physics, The LNM institute for Information Technology, Jamdoli, 302031 Jaipur, India*
E-mail: gdsharma273@gmail.com
https://www.lnmiit.ac.in/Department/Physics/Physics_ContactNew.htm
[‡] These authors contributed equally to this work.

remarkably efficient sensitizers in DSSCs.[11] Another key factor is the incorporation of an electron-withdrawing spacer between the porphyrin ring and the anchoring group. This can alter the properties of the chromophore (i.e., lower HOMO–LUMO gap, wider absorption), resulting in better device performance.[9c,10b,11e,12] Dye aggregation is frequently observed in porphyrin-based DSSCs, and it is detrimental to device performance, as it enables intermolecular charge recombination. Numerous studies reported that porphyrins containing long alkoxy chains, either at the periphery or at the electron-withdrawing spacer, were capable of preventing the formation of aggregates.[11c,13] Thus, the introduction of an anchoring group and alkoxy chains along with the incorporation of a spacer promoting the electron-transfer process could significantly enhance the performance of porphyrin derivatives in DSSCs.

To this end, we synthesized two novel Zn^{II}–porphyrin sensitizers, namely, ZnP(SP)CNCOOH and ZnPCNCOOH, as shown in Schemes 1 and 2, respectively. Both porphyrins contain cyanoacrylic acid as the anchoring group for efficient attachment onto the semiconductor (TiO_2) surface. In the case of ZnPCNCOOH, the anchoring group is directly linked to one of the macrocycle's four *meso*-phenyl rings, whereas in ZnP(SP)CNCOOH a π spacer (SP) bearing two polyethylene glycol chains is inserted between the macrocycle and the anchoring group. The π spacer allows better electronic communication between the macrocycle and the anchoring group, whereas the polyethylene glycol chains are used to prevent dye aggregation. This hypothesis is supported by density functional theory (DFT) calculations, which also indicate that ZnP(SP)CNCOOH is expected to act as a more efficient photosensitizer owing to its large dipole moment. DSSCs sensitized by both porphyrins were fabricated, and the photovoltaic performance (power conversion efficiency, PCE) of ZnP(SP)CNCOOH is found to be twofold higher than that of solar cells based on ZnPCNCOOH.

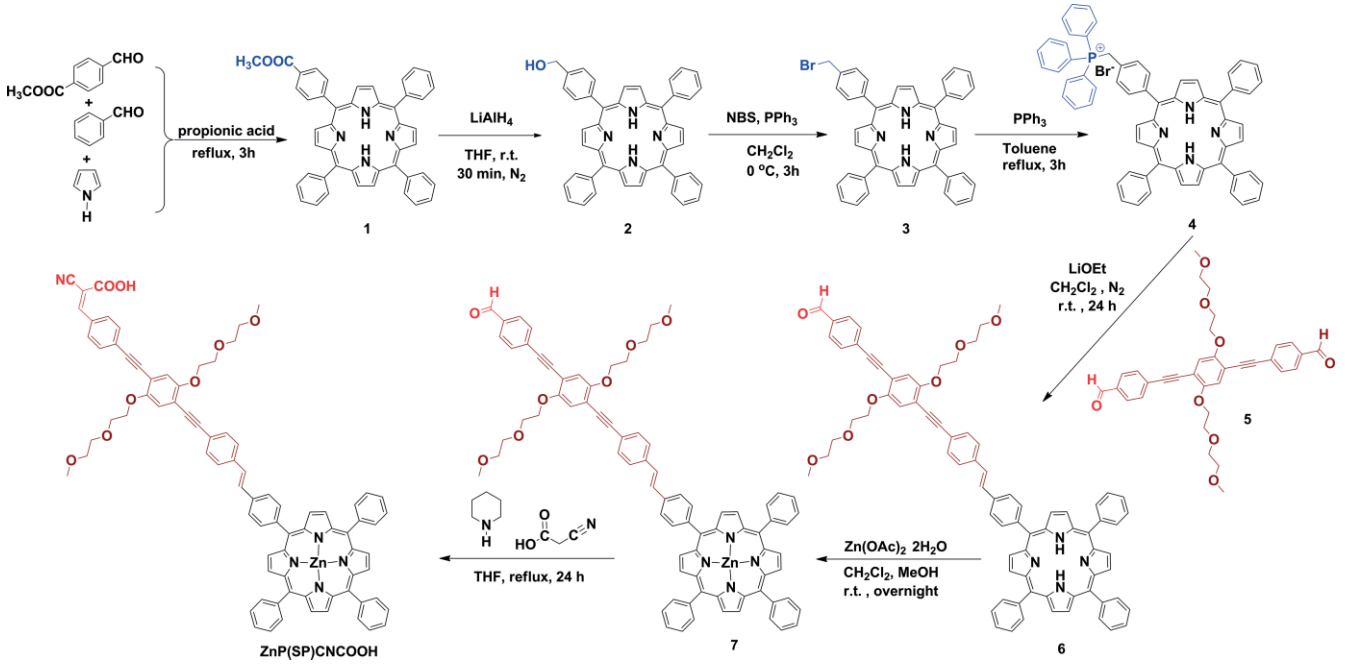

Scheme 1. Synthetic procedure for compound ZnP(SP)CNCOOH.

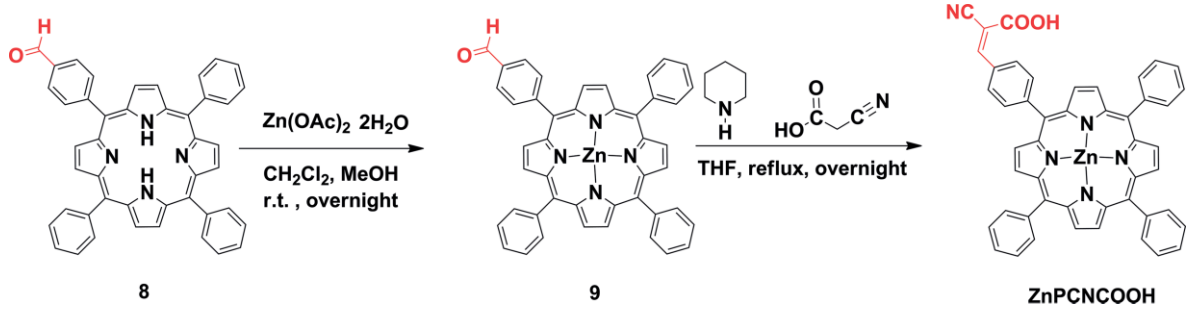

Scheme 2. Synthetic procedure for compound ZnPCNCOOH.

Results and Discussion

Synthesis and Characterization

The procedures followed for the preparation of compounds ZnP(SP)CNCOOH and ZnPCNCOOH are outlined in Schemes 1 and 2, respectively. For the synthesis of ZnP(SP)CNCOOH, porphyrin derivative **1** was initially prepared by condensation of methyl 4-formylbenzoate, benzaldehyde, and pyrrole in propionic acid. Then, reduction with $LiAlH_4$ produced compound **2**, which was subsequently treated with *N*-bromosuccinimide (NBS) to give bromo-substituted porphyrin **3**. Compound **3** was heated at reflux with triphenylphosphine to produce phosphonium ylide porphyrin **4**, which then underwent a Wittig reaction along with aldehyde **5**[14] to yield derivative **6**. Afterwards, the porphyrin ring was metalated with zinc to form derivative **7**, and finally, a Knoevenagel condensation was performed with 2-cyanoacetic acid to obtain the desired product, ZnP(SP)CNCOOH, in 43 % yield.

Accordingly, for the synthesis of porphyrin ZnPCNCOOH, the first step involved the metalation of formyl-substituted porphyrin **8**[15] with zinc to yield corresponding zinc–porphyrin **9**. Finally, a Knoevenagel condensation between derivative **9** and 2-cyanoacetic acid was performed to afford ZnPCNCOOH in 56 % yield.

All compounds were fully characterized by ^1H NMR and ^{13}C NMR spectroscopy (Figures S1–S25 in the Supporting Information) and MALDI-TOF mass spectrometry. Notably, the ^1H NMR spectra of intermediate derivatives **6** and **7**, as well as that of the final ZnP(SP)CNCOOH product, confirm the *E* configuration of the newly formed double bond (J = 16–16.5 Hz) for the AB system corresponding to the vinylic protons. Furthermore, in both final dyes [ZnP(SP)CNCOOH and ZnPCNCOOH] the successful addition of the cyanoacrylic acid unit is confirmed by their ^1H NMR and ^{13}C NMR spectra. More specifically, in the ^1H NMR spectra of ZnP(SP)CNCOOH and ZnPCNCOOH singlets appear at δ = 8.14 and 8.53 ppm, respectively, and they can be attributed to the protons of the double bonds, whereas in the ^{13}C NMR spectrum of ZnPCNCOOH the characteristic resonances of the –CN (δ = 117.8 ppm) and –COOH (δ = 163.2 ppm) groups are present.

Single-Crystal X-ray Diffraction Study

Single crystals, suitable for X-ray crystallographic analysis, of intermediate porphyrin **4** were obtained by slow evaporation of a dichloromethane/hexane (1:1, *v*/*v*) solution of the compound. The crystal structure and refinement parameters are given in the Supporting Information (text and Table S1), whereas a view of the molecular structure, together with selected bond lengths and angles, are given in Figure S26 (full list of bond lengths and angles are provided in Tables S2–S5).

Photophysical Properties

The photophysical characterization of the final compounds [ZnP(SP)CNCOOH and ZnPCNCOOH] was performed by absorption spectroscopy both in solution and in films adsorbed onto TiO_2. In Figure 1, the UV/Vis absorption spectra of the final dyes are presented, and typical features for zinc–porphyrin derivatives are observed for both compounds.[16] For both porphyrin dyes one strong absorption band (Soret band) is present at 428 nm in the case of ZnPCNCOOH and at 422 nm for ZnP(SP)CNCOOH, along with two Q bands located in the 540–610 nm region. Particularly, ZnPCNCOOH exhibits two Q bands at 561 and 601 nm, whereas ZnP(SP)CNCOOH exhibits these bands at 548 and 587 nm. A summary of the absorption data along with the absorption coefficients for both porphyrin derivatives is provided in Table S6.

Upon adsorption of the ZnP(SP)CNCOOH and ZnPCNCOOH porphyrins onto TiO_2 films, their corresponding UV/Vis absorption bands appear to be significantly broader and redshifted

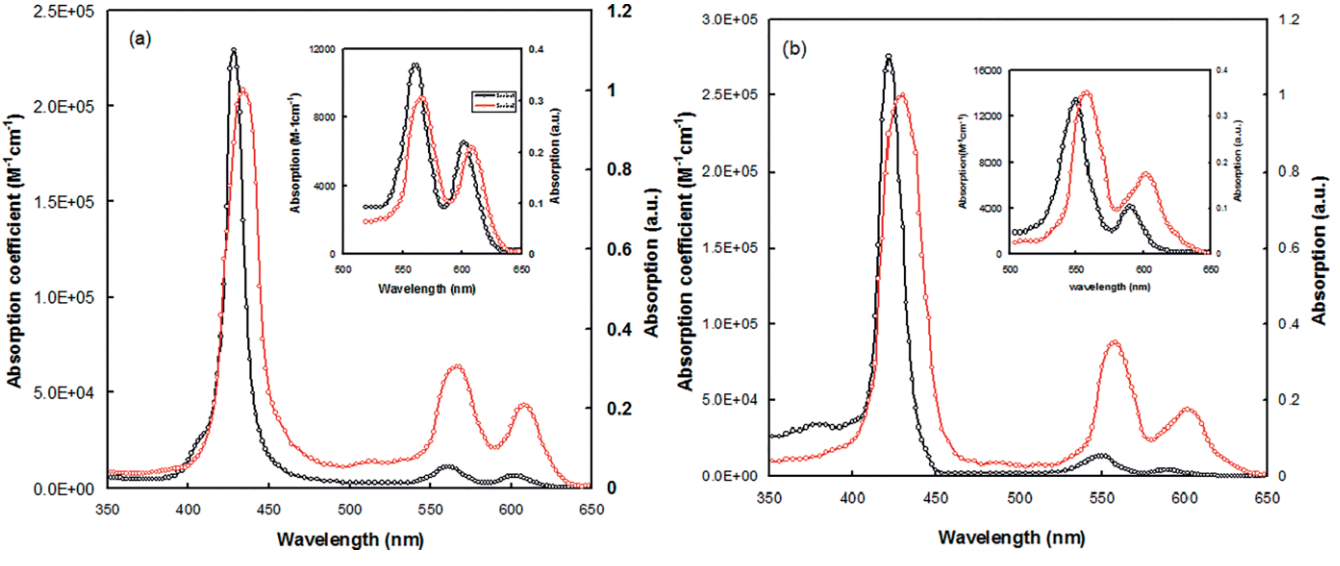

Figure 1. UV/Vis absorption spectra of the (a) ZnPCNCOOH (**1**) and (b) ZnP(SP)CNCOOH (**2**) porphyrin dyes in solution (black) and adsorbed onto TiO_2 films (red).

relative to those in solution (Figure 1a,b). This broadening may be attributed to intra- or intermolecular interactions between the porphyrin dyes and TiO_2, which enhance light harvesting in the far near red region.[17]

Using the onset absorption edge, λ_{onset}, of the Q band of the absorption spectra in films and the expression $E_{gopt} = 1240/\lambda_{onset}$, the optical band gaps of ZnP(SP)CNCOOH and ZnPCNCOOH were found to be 1.90 and 1.94 eV, respectively.

Electrochemical Studies

The electrochemical properties of ZnP(SP)CNCOOH and ZnPCNCOOH were investigated by cyclic and square-wave voltammetry measurements (Figure S27). Both dyes exhibit two reversible oxidations and two reversible reductions, and their potentials are presented in Table 1. The first oxidation potentials of ZnP(SP)CNCOOH and ZnPCNCOOH, corresponding to their HOMO energy levels, are found at 1.06 and 1.07 V (vs. SCE), respectively. The HOMOs of both photosensitizers are more positive than the redox potential of I_3^-/I^-. Consequently, all oxidized dyes can be regenerated by the reducing species of the electrolyte, considering that the reduction potential for the I_3^-/I^- redox couple is 0.40 V (vs. SCE). In addition, the LUMO energy levels of ZnP(SP)CNCOOH and ZnPCNCOOH, corresponding to their first reduction potentials, are at –1.28 and –1.29 V (vs. SCE), respectively. The reduction potentials are more negative than the conduction band (CB) of TiO_2 (–0.74 V vs. SCE). This implies an effective electron-injection process from the excited dyes into the CB of TiO_2.

DFT Studies

Density functional theory (DFT) calculations were performed to shed light onto the molecular structures and the electronic properties of the two final porphyrin dyes. The gas-phase-optimized coordinates of ZnPCNCOOH and ZnP(SP)CNCOOH are listed in Tables S7 and S8, respectively, whereas two different views of their corresponding structures are illustrated in Figures 2 and S28. In both cases, it can be noted that all four peripheral phenyl rings are almost perpendicular to the porphyrin macrocycle, whereas the central zinc ion is coplanar to the four pyrrole rings. Furthermore, in the optimized geometry we observe that the phenyl rings of the π-spacer group are nearly perpendicular to the porphyrin core, and they simultaneously adopt a coplanar orientation to each other. The polyethylene glycol chains on the second phenyl substituent of the π-spacer are extended above and under the plane of the dye, which thus reduces the probability of dye aggregation onto the TiO_2 surface as a result of π–π stacking. The frontier molecular orbitals (FMOs) as well as the energy contributions corresponding to ZnPCNCOOH and ZnP(SP)CNCOOH are depicted in Figures S29 and S30, respectively. As it can be clearly seen, in both derivatives the electron-density distributions of the HOMOs are predominantly spread over the porphyrin macrocycle. In ZnPCNCOOH, some additional contributions can be found on the peripheral phenyl rings, whereas in the case of ZnP(SP)CNCOOH part of the electron density is located at the spacer's phenyl unit bearing the polyethylene glycol chains (HOMO–2). In a similar manner, the electron densities of the LUMO orbital of both final compounds are localized on the anchoring group, whereas in the other two orbitals (LUMO+1 and LUMO+2) the electron densities are mainly spread over the porphyrin macrocycle and the peripheral units with minor contributions to the cyanoacrylic acid. On the basis of the aforementioned findings, it is safe to assume that intramolecular electron transfer is favored in both ZnPCNCOOH and ZnP(SP)CNCOOH and that they can be considered as promising sensitizers for

Table 1. Electrochemical redox data for ZnP(SP)CNCOOH and ZnPCNCOOH in THF.[a]

Dye	E^1_{ox} (V vs. SCE)	E^2_{ox} (V vs. SCE)	E^1_{red} (V vs. SCE)	E^2_{red} (V vs. SCE)	H–L gap (expt) (eV)
ZnP(SP)CNCOOH	1.06	1.32	–1.28	–1.46	2.34
ZnPCNCOOH	1.07	1.32	–1.29	–1.61	2.36

[a] All potentials are reported vs. SCE, and ferrocene/ferrocenium (Fc/Fc^+) was used as the internal standard ($E^{ox}_{1/2}$ = 0.60 V)..

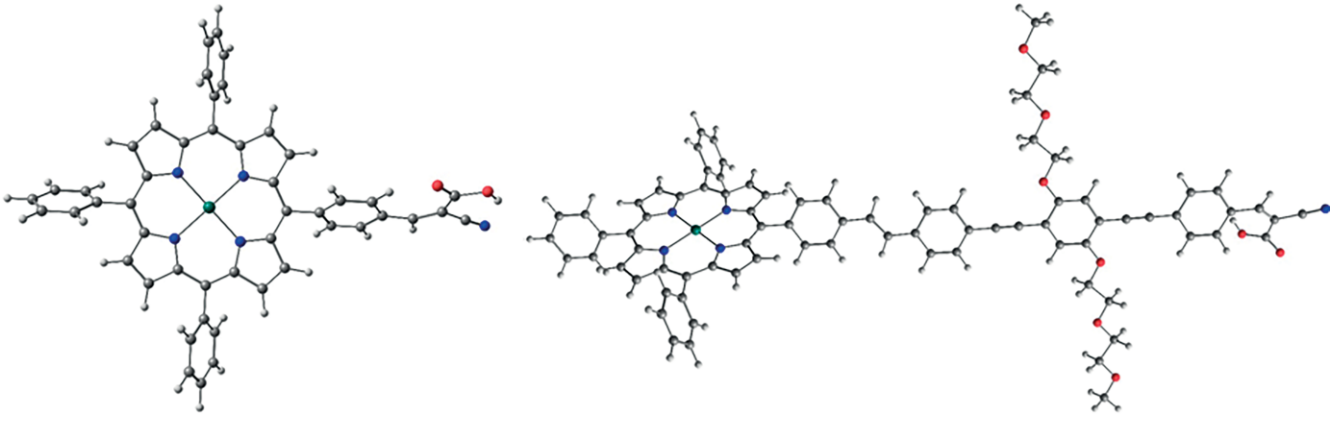

Figure 2. Gas-phase-geometry-optimized structures of ZnPCNCOOH (left) and ZnP(SP)CNCOOH (right). Carbon, nitrogen, hydrogen, oxygen, and zinc correspond to gray, blue, white, red, and green spheres, respectively.

DSSC applications. Noteworthy, the dipole moment (μ) of ZnP(SP)CNCOOH (13.51 D) is considerably larger than that of ZnPCNCOOH (7.40 D). According to previously published studies, dyes that present larger μ values normally reach higher power conversion efficiencies (PCEs) if applied in DSSCs.[16a,18] This hypothesis is further supported by the photovoltaic parameters recorded for the cells based on both sensitizers. More specifically, the PCE value is significantly higher in the case of ZnP(SP)CNCOOH (7.61 %) than in the case of ZnPCNCOOH (5.02 %). Moreover, the calculated HOMO and LUMO energy values, along with the theoretically calculated HOMO–LUMO (H–L) gap and the dipole moment (μ) of the two final porphyrin derivatives are summarized in Table S9. The theoretically calculated H–L gaps [2.344 eV for ZnPCNCOOH and 2.173 eV for ZnP(SP)CNCOOH] were determined by using THF as the solvent, and they were found to be in close agreement with the corresponding experimentally obtained H–L gaps that were derived through electrochemical studies (Table 1).

DSSC Performance

The photovoltaic performance of DSSCs sensitized by ZnP(SP)CNCOOH and ZnPCNCOOH were investigated under illumination (AM 1.5G, 100 mW cm^{-2}). An electrolyte consisting of 0.3 M 1,2-dimethyl-3-propylimidazolium iodide (DMPII), 0.1 M LiI, 0.05 M I_2, and 0.5 M 4-*tert*-butylpyridine (4-TBP) in acetonitrile was used. Chenodeoxycholic acid (CDCA) (2 mM) was also added as a co-adsorbent, as it can hinder dye aggregation onto the TiO_2 surface. The current–voltage (*J*–*V*) characteristics of the two DSSCs are shown in Figure 3a, whereas the corresponding photovoltaic parameters are summarized in Table 2. The solar cells sensitized by ZnPCNCOOH reach an overall PCE value of 5.02 % with a short-circuit current (J_{sc}) of 11.04 mA cm^{-2}, an open-circuit voltage (V_{oc}) of 0.67 V, and a fill factor (FF) of 0.68, whereas the solar cells based on ZnP(SP)CNCOOH display a higher PCE of 7.61 % and enhanced photovoltaic characteristics, that is, J_{sc} = 14.49 mA cm^{-2}, V_{oc} = 0.73 V, and FF = 0.72. This clearly indicates that the incorporation of the π-spacer between the porphyrin (donor) unit and the cyanoacrylic acid (acceptor) group significantly improves the overall performance of ZnP(SP)CNCOOH.

Table 2. Photovoltaic parameters of DSSCs sensitized with ZnP(SP)CNCOOH and ZnPCNCOOH dyes.

Sensitizer	J_{sc} (mA cm^{-2})	V_{oc} (V)	FF	PCE (%)
ZnP(SP)CNCOOH (**2**)	14.49	0.73	0.72	7.61
ZnPCNCOOH (**1**)	11.04	0.67	0.68	5.02

The effect of the π-conjugated bridge on the DSSC performance was further investigated by measuring the incident photon to current conversion efficiency (IPCE) spectra. As shown in Figure 3b, both porphyrins can effectively convert light into a photocurrent over a wide UV/Vis spectral region. The IPCE spectra of the two solar cells closely resemble the absorption spectra of the corresponding porphyrin sensitizers. The band that is located in the 400–440 nm range in both DSSCs reaches a similar peak value of approximately 63 %. On the other hand, the solar cell sensitized by ZnP(SP)CNCOOH achieves higher peak values in the two bands in the 520–620 nm region. In general, the IPCE spectrum of the ZnP(SP)CNCOOH-based device is broader than that of the ZnPCNCOOH-based device, which leads to a significantly higher J_{sc} value. The integrated values of J_{sc} for the solar cells based on ZnPCNCOOH and ZnP(SP)CNCOOH, as calculated from their corresponding IPCE spectra, are 10.91 and 14.36 mA cm^{-2}, respectively, which are consistent with the values measured in their experimental *J*–*V* characteristics.

To obtain more information about the differences in the J_{sc} values and the IPCE responses of the two solar cells, the light-harvesting efficiencies (LHEs) were evaluated. The transmittance spectra of their corresponding TiO_2 films with a thickness of 8 μm, upon using 0.2 mM solutions of the dyes, were measured. As shown in Figure 4, in the case of ZnP(SP)CNCOOH a higher LHE was calculated covering almost 90 % of the entire wavelength region (400–670 nm). On the contrary, ZnPCNCOOH adsorbed onto TiO_2 exhibited lower LHE with a narrower coverage window (400–620 nm), which is in agreement with the observed J_{sc} values and the IPCE spectra.[19]

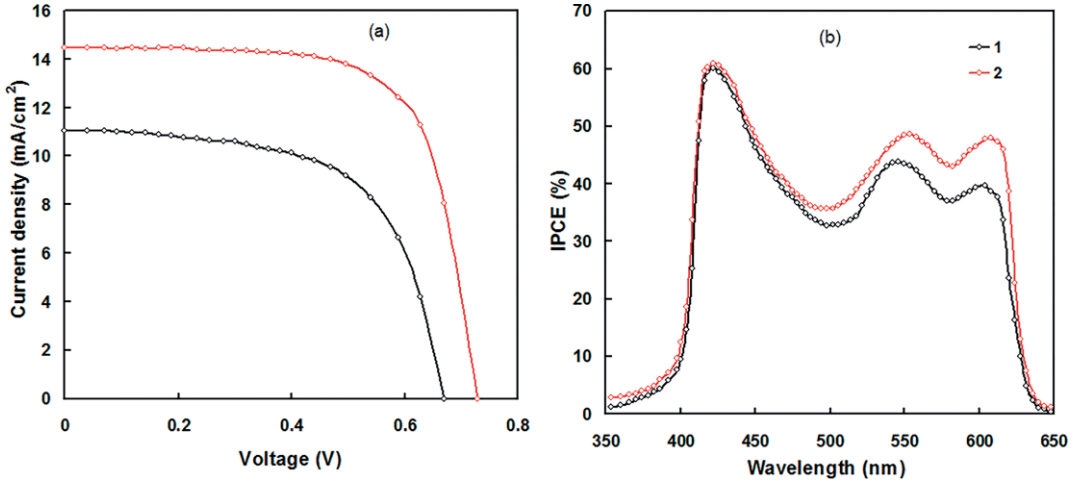

Figure 3. (a) Current–voltage (*J*–*V*) characteristics under illumination and (b) IPCE spectra of DSSCs based on ZnP(SP)CNCOOH (**2**) and ZnPCNCOOH (**1**).

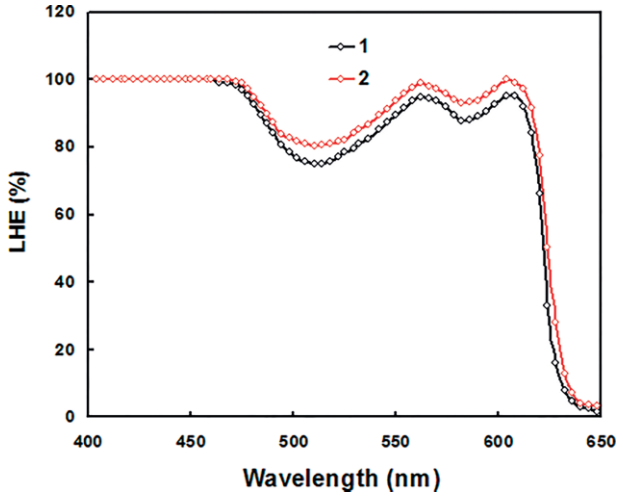

Figure 4. LHE spectra of dye-loaded TiO_2 films.

In general, the LHE can be enhanced either by increasing the dye loading onto TiO_2 or by increasing the molar extinction coefficient of the dye.[20] Dye loading values for the two devices based on either ZnPCNCOOH or ZnP(SP)CNCOOH were calculated by measuring the absorption spectra of solutions containing amounts of unbound dye molecules that were detached from the semiconductor surface. Particularly, after the attachment of porphyrins onto TiO_2, the modified films were washed to remove the unbound porphyrin derivatives. The dye loading values were found to be 2.14×10^{-7} and 2.62×10^{-7} mol cm^{-2} for ZnPCNCOOH and ZnP(SP)CNCOOH, respectively. Given that there is a very small difference between these values, it can be concluded that the high LHE of the ZnP(SP)CNCOOH-sensitized DSSC originates from the strong light-absorbing ability of the dye.[21] Another important parameter that affects the LHE of a porphyrin-sensitized solar cell is the total area of the Q-absorption band estimated by the integral $\int \varepsilon(\nu) d\nu$, in which ε is the molar extinction coefficient and ν is the wavenumber. Indeed, the integrals $\int \varepsilon(\nu) d\nu$ for DSSCs based on ZnPCNCOOH and ZnP(SP)CNCOOH were found to be 28.6×10^6 and 19.5×10^6 M^{-1} cm^{-1}, respectively.

To gain insight into the charge-transfer processes and recombination dynamics of the constructed DSSCs, electrochemical impedance spectroscopy (EIS) in the dark was employed. Also, to determine the interfacial charge recombination resistance (R_{cr}), effective capacitance (C_μ), and electron lifetime (τ_n), measurements were conducted.[19–21] The applied voltage was around −0.7 V and was scanned from 10^5 to 0.1 Hz. The Nyquist and EIS plots of the DSSCs are shown in Figure 5a. In general, these plots consist of three semicircles that are associated with charge transfer at the counter electrode/electrolyte interface (high-frequency region), electron-transfer kinetics at the TiO_2/dye/electrolyte interface (middle-frequency region), and Nernstian diffusion of I_3^-/I^- (low-frequency region).[22] The radius of the semicircle of the Nyquist plots in the high-frequency region is larger for the DSSC based on ZnP(SP)CNCOOH than the DSSC based on ZnPCNCOOH, indicating a larger resistance of the charge-transfer process at the counter electrode/electrolyte interface (R_{ce}) in the case of ZnP(SP)CNCOOH.[23] This can be attributed to the different distribution and velocity of the electrolyte as well as the different molecular geometry and intermolecular packing of the dye onto TiO_2.[21,24] The large semicircle observed in the middle-frequency region represents the charge recombination resistance (R_{rec}) at the TiO_2/dye/electrolyte interface, which is inversely proportional to the rate of recombination. The radius of this circle is larger for ZnP(SP)CNCOOH than for ZnPCNCOOH, indicating an increased R_{rec} value, which suppresses the recombination rate. Moreover, the C_μ value of ZnP(SP)CNCOOH (342 μF cm^{-2}) is lower than that of ZnPCNCOOH (315 μF cm^{-2}), and this suggests a possible positive shift in the TiO_2 conduction band edge. In addition, the τ_n values can be calculated from the peak frequency (f_{max}) in the lower-frequency region from the Bode phase plots (Figure 5b) of the two DSSCs, according to the expression[25] $\tau_n = 1/(2\pi f_{max})$, and they were found to be 29.62 and 19.13 ms for ZnP(SP)CNCOOH and ZnPCNCOOH, respectively. The higher R_{rec} and τ_n values for the DSSC based on ZnP(SP)CNCOOH indicate that charge transfer from TiO_2 back to the oxidized dye and the redox couple is slower. These contradictory sequences (a positive shift in the TiO_2 conduction band edge leads to a decrease in V_{oc}) reveal that the relatively high V_{oc} value for the

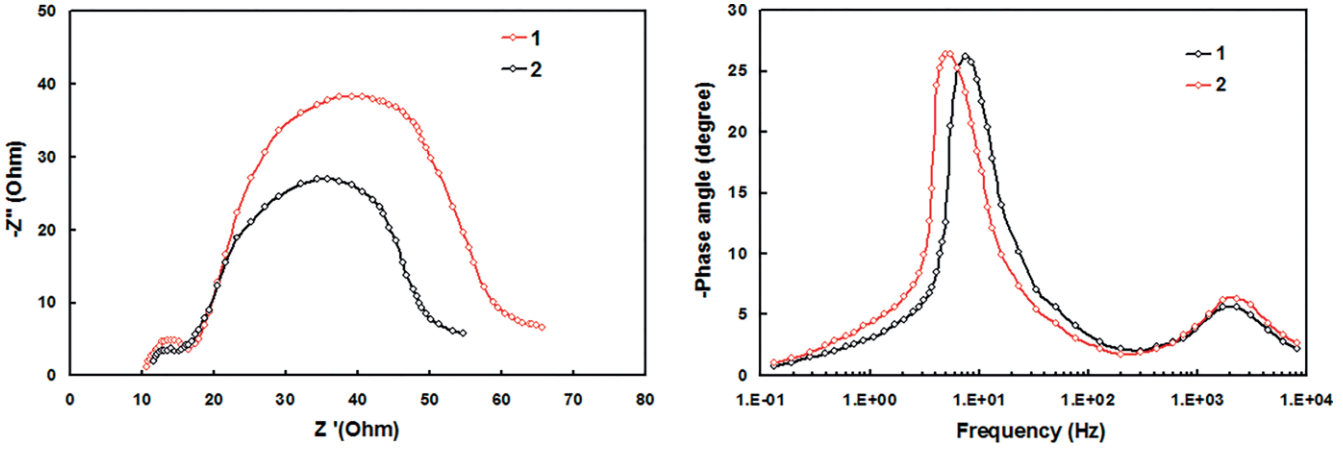

Figure 5. (a) Nyquist plots and (b) Bode phase plots of DSSCs based on the ZnPCNCOOH (**1**) and ZnP(SP)CNCOOH (**2**) porphyrin dyes.

ZnP(SP)CNCOOH-sensitized DSSC is attributed to suppressed charge recombination rather than a shift in the TiO_2 conduction band.[19] The higher R_{rec} and τ_n values for the ZnP(SP)CNCOOH-sensitized DSSC indicate that its greater J_{sc} and PCE values may arise from the considerably suppressed charge recombination.

We also measured the charge-transport resistance (R_d) for both DSSCs from the Nyquist and EIS plots under illumination, and the values are 25.04 $\Omega\,cm^2$ for ZnPCNCOOH and 20.16 $\Omega\,cm^2$ for ZnP(SP)CNCOOH. The R_d and R_{rec} values of a DSSC are related to the τ_n and electron-transport time (τ_d) [which is a measure of the average time taken by the injected electron to reach the fluorine-doped tin oxide (FTO) electrode] according to the relationship:

$$\frac{\tau_d}{\tau_n} = \frac{R_d}{R_{rec}}$$

The τ_d value of the ZnP(SP)CNCOOH-based DSSC (12.14 ms) is lower than that of the ZnPCNCOOH-based DSSC (16.39 ms). The faster electron transport is associated with its higher J_{sc} and indicates that the electrons are collected at the photoanode at a faster rate. Finally, the J_{sc} of a DSSC is highly dependent on its charge-collection efficiency (η_{cc}), which is calculated according to the relationship:[26]

$$\eta_{cc} = \left(1 + \frac{\tau_d}{\tau_n}\right)^{-1}$$

The η_{cc} value for the solar cell sensitized with ZnP(SP)CNCOOH (69 %) is higher than that for the solar cell sensitized with ZnPCNCOOH (54 %), and ultimately, this leads to improved J_{sc} and PCE values. These results indicate that the porphyrin dye bearing polyethylene glycol side chains favors slow charge recombination along with faster charge extraction.

It is evident from the IPCE spectra (Figure 3b) that the IPCE values for the DSSC based on ZnP(SP)CNCOOH are higher than those recorded for the DSSC based on ZnPCNCOOH, particularly in the Q bands. The IPCE of the DSSC is the product of three parameters, namely, LHE, electron-injection efficiency from the excited dye into the CB of the TiO_2 (ϕ_{inj}), and η_{cc}, described as:

$$IPCE\ (\lambda) = LHE \times \phi_{inj} \times \eta_{cc}$$

As discussed above, ZnP(SP)CNCOOH-based DSSCs present higher LHE. The ϕ_{inj} in DSSCs depends on the energy difference between the LUMO of the dye and the conduction band of the semiconductor. As can be seen from the energy-band diagram (Figure 6), this difference is similar for both cells; hence, we can assume that the electron-injection efficiency is almost the same. Owing to the higher LHE for the ZnP(SP)CNCOOH-based DSSC (Figure 4), more electrons are probably injected into the conduction band of TiO_2 from the excited state of ZnP(SP)CNCOOH. The value of η_{cc} for the ZnP(SP)CNCOOH-based DSSC is higher than that for the ZnPCNCOOH-based DSSC, resulting in improved IPCE values.

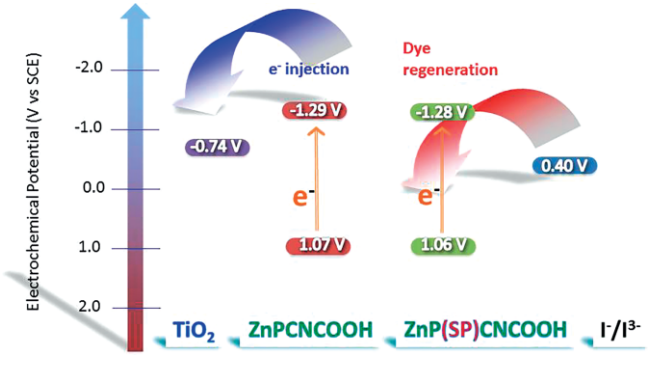

Figure 6. Electron injection into TiO_2 and regeneration in solar cells based on the ZnPCNCOOH and ZnP(SP)CNCOOH dyes are presented in the electrochemical potential diagram [V].

Conclusions

In this report, the synthesis of two new porphyrin dyes, namely, ZnPCNCOOH and ZnP(SP)CNCOOH, and their study as sensitizers in DSSCs were presented. Both porphyrins were adsorbed onto the TiO_2 surface through cyanoacrylic acid anchoring groups. Moreover, in the case of ZnP(SP)CNCOOH a π-conjugated spacer was introduced between the porphyrin and the anchoring group, which improved their electronic communication and suppressed their undesired aggregation on the TiO_2 surface. Both derivatives were fully characterized by NMR and UV/Vis spectroscopy and MALDI-TOF mass spectrometry. DFT calculations along with cyclic voltammetry experiments showed that both dyes possess appropriate HOMO and LUMO levels for their application in DSSCs. ZnP(SP)CNCOOH- and ZnPCNCOOH-based solar cells were constructed, and they showed PCE values of 7.61 and 5.02 %, respectively. The higher PCE value of ZnP(SP)CNCOOH was attributed to its enhanced short-circuit current (J_{sc}) under illumination, its longer electron lifetime (τ_n), and higher charge recombination resistance (R_{rec}).

Experimental Section

Materials and Techniques: Reagents and solvents were purchased as reagent grade from usual commercial sources and were used without further purification, unless otherwise stated. Thin-layer chromatography was performed on silica gel 60 F_{254} plates, whereas chromatographic separations were performed by using silica gel 60, SDS, 70–230 mesh ASTM. ^1H NMR and ^{13}C NMR spectra were recorded with Bruker AMX-500 MHz and Bruker DPX-300 MHz spectrometers as solutions in deuterated solvents by using the solvent signal as the internal standard. High-resolution mass spectra were recorded with a Bruker ultrafleXtreme MALDI-TOF/TOF spectrometer by using *trans*-2-[3-(4-*tert*-butylphenyl)-2-methyl-2-propenylidene]malononitrile as the matrix.

X-ray Crystallography

Suitable single crystals of compound **4** were protected with paratone-N and mounted for data collection on a STOE IPDS II diffractometer equipped with a Mo-K_α sealed-tube X-ray source (λ = 0.71073 Å, graphite monochromated) and an image plate detector. Data collection, data reduction, integration, and cell-parameter determination were performed by using the STOE X-AREA package software,[27] whereas a numerical absorption correction was also applied by using the STOE X-RED[28] and X-SHAPE software packages.[29] The structure was solved by direct methods and was implemented in SHELXS-2014,[30] which allowed immediate location of most of the heaviest atoms. The remaining non-hydrogen atoms were located from difference Fourier maps calculated from succes-

sive full-matrix least-squares refinement cycles on F^2 by using SHELXL-2014.[31] All structural refinements were performed by using the graphical interface ShelXle.[30a] All non-hydrogen atoms were successfully refined by using anisotropic displacement parameters. The PLATON SQUEEZE[32] procedure was applied to recover 64 electrons per unit cell in one void (total volume 576 Å^3), that is, 16 electrons per formula unit. Lattice water (10 electrons/H_2O) was present, and therefore, the electrons recovered by SQUEEZE were assigned as 1.5 H_2O molecules per formula unit.

CCDC 1819581 (for **4**) contains the supplementary crystallographic data for this paper. These data can be obtained free of charge from The Cambridge Crystallographic Data Centre.

Photophysical Measurements: UV/Vis absorption spectra were measured with a Shimadzu UV-1700 spectrophotometer by using 10 mm path-length cuvettes.

Electrochemistry: Cyclic and square-wave voltammetry experiments were performed at room temperature by using an AutoLab PGSTAT20 potentiostat and appropriate routines available in the operating software (GPES version 4.9). All measurements were performed in freshly distilled and deoxygenated tetrahydrofuran (THF) with a solute concentration of about 1.0 mM in the presence of tetrabutylammonium tetrafluoroborate (0.1 M) as a supporting electrolyte. A three-electrode cell setup was used with a platinum working electrode, a saturated calomel electrode (SCE) as the reference electrode, and a platinum wire as the counter electrode. All potentials are reported versus the ferrocene/ferrocenium couple (0.60 V vs. SCE under the above conditions).

Computational Details: Density functional theory (DFT) calculations[33] were performed with the B3LYP/6-31G(d)[34] level of theory by using the GAUSSIAN 03 program suite.[35] For all the gas-phase geometry optimizations, the LANL2DZ basis set was selected for Zn atoms and the 6-31G(d) basis set was used for lighter atoms. To guarantee the absence of imaginary frequencies, the optimized minimum-energy structures were subjected to vibrational frequency analysis calculations. Tomasi's polarizable continuum model (PCM)[36] was applied to describe the solvent effect (tetrahydrofuran) with standard dielectric constant $e = 7.426$. The output geometries and molecular orbitals of ZnPCNCOOH and ZnP(SP)CNCOOH were visualized by using ChemCraft software (version 1.6).[37]

DSSC Fabrication and Characterization

For fabrication of the DSSCs, the transparent fluorine-doped tin oxide (FTO) glass substrates (10 Ω sq^{-1}) were first successively cleaned in detergent solution, deionized water, ethanol, and acetone by using an ultrasonic bath for 20 min and were then dried under ambient conditions. Details of the fabrication of the photoanode are described in our earlier work.[16a] The adsorption of the porphyrin dyes on TiO_2 was performed with 0.4 mM dye solution in THF/EtOH (1:4) for 12 h at room temperature. The counter electrode was prepared by spin coating of a H_2PtCl_4 solution (0.002 g in 1 mL *i*PrOH) onto a precleaned FTO-coated glass substrate and then heating at 450 °C for 15 min in air. The sensitized working electrode was assembled with the Pt-coated FTO electrode into a sandwich-type cell and was sealed with the hot-melt polymer Surlyn as a spacer between the electrodes. To complete the fabrication of the DSSC, the electrolyte composed of 0.3 M DMPII, 0.1 M LiI, 0.05 M I_2, and 0.5 M 4-*tert*-butylpyridine in CH_3CN was introduced into the space between the two electrodes through a predrilled hole in the platinum-coated FTO by vacuum backfilling. The amounts of dye loaded were determined by dye desorption in a basic solution (0.1 M NaOH in THF/H_2O = 1:1) followed by spectroscopic measurements.

The current–voltage (*J*–*V*) characteristics of the DSSCs under illumination were measured by a Keithley source meter, a solar simulator coupled with a 150 W xenon lamp, and an AM optical filter to give 100 mW cm^{-2} illumination at the DSSC surface. The active area of the DSSCs was 0.20 cm^2. Incident photon to current conversion efficiency (IPCE) data were obtained as a function of different wavelengths by using a xenon lamp, a monochromator, and a Keithley source meter under constant illumination intensity at each wavelength. Intensity calibration for IPCE data was performed by using a standard silicon photodiode. Current was measured under short-circuit conditions. Electrochemical impedance (EI) spectra, in the dark, were recorded by using an electrochemical workstation (Autolab PGSTAT) with a frequency response analyzer. A frequency range of 10 mHz to 100 kHz and an alternating current potential of 10 mV were used. A direct-current bias equivalent to the open-circuit voltage of the DSSC was applied. Electrochemical impedance spectroscopy (EIS) data were analyzed by using Z-View software with an appropriate equivalent circuit.

5-[4-(Methoxycarbonyl)phenyl]-10,15,20-triphenylporphyrin (1): A propionic acid (40.0 mL) solution of benzaldehyde (0.70 mL, 6.9 mmol) and methyl 4-formylbenzoate (377 mg, 2.3 mmol) was added to a round-bottomed flask. The mixture was heated to 100 °C and then pyrrole (0.64 mL, 9.20 mmol) was added dropwise. The mixture was heated at reflux whilst stirring for 3 h, protected from light. The solution was cooled to room temperature, and then H_2O was added. The mixture was filtered, and the precipitate was washed with water (100 mL). The crude residue was purified by column chromatography (silica gel, CH_2Cl_2/hexane, 2:3) to obtain porphyrin **1** as a dark purple solid. Yield: 240 mg (16 %). ^{1}H NMR (300 MHz, $CDCl_3$): δ = 8.87 (m, 6 H), 8.80 (d, J = 4.8 Hz, 2 H), 8.45 (d, J = 8.1 Hz, 2 H), 8.32 (d, J = 8.1 Hz, 2 H), 8.23 (m, 6 H), 7.76 (m, 9 H), 4.12 (s, 3 H), –2.76 (s, 2 H) ppm. ^{13}C NMR (75 MHz, $CDCl_3$): δ = 167.5, 147.2, 142.18, 142.15, 134.72, 134.68, 131.4, 129.7, 128.0, 127.9 126.86, 126.85, 120.7, 120.5, 118.7, 52.6 ppm. HRMS (MALDI-TOF): calcd. for $C_{46}H_{32}N_4O_2$ 672.2525 [M]$^+$; found 672.2532.

5-[4-(Hydroxymethyl)phenyl]-10,15,20-triphenylporphyrin (2): $LiAlH_4$ (18 mg, 0.38 mmol) was added to a solution of **1** (65 mg, 0.096 mmol) in anhydrous THF (10 mL), and the mixture was stirred at room temperature. After stirring for 30 min, H_2O and then an aqueous solution of NaOH (15 %, *w*/*v*) was very carefully poured into the mixture to neutralize $LiAlH_4$. CH_2Cl_2 was added, and the organic layer was washed with saturated $NaHCO_3$ solution. The organic solvents were evaporated under reduced pressure, and the product was purified by column chromatography (silica gel, CH_2Cl_2) to obtain porphyrin **2** as a purple solid. Yield: 43 mg (70 %). ^{1}H NMR (500 MHz, $CDCl_3$): δ = 8.86 (s, 8 H), 8.22 (m, 8 H), 7.77 (m, 11 H), 5.05 (s, 2 H), –2.76 (s, 2 H) ppm. ^{13}C NMR (75 MHz, $CDCl_3$): δ = 142.3, 141.6, 140.5, 134.9, 134.7, 131.2, 127.9, 126.8, 125.4, 120.3, 119.9, 65.4 ppm. HRMS (MALDI-TOF): calcd. for $C_{45}H_{32}N_4O$ 644.2576 [M]$^+$; found 644.2568.

5-[4-(Bromomethyl)phenyl]-10,15,20-triphenylporphyrin (3): A solution of porphyrin **2** (32 mg, 0.050 mmol) and PPh_3 (54 mg, 0.205 mmol) in CH_2Cl_2 (10 mL) was cooled to 0 °C. Then, NBS (36 mg, 0.200 mmol) was added, and the mixture was stirred at 0 °C for 3 h, protected from light. The green solution was washed with saturated $NaHCO_3$ solution until it became red and once with H_2O. The organic layer was then dried (Na_2SO_4), and the solvent was evaporated under reduced pressure. The product was purified by column chromatography (silica gel, CH_2Cl_2/hexane, 3:2) to obtain purple porphyrin **3**. Yield: 30 mg (85 %). ^{1}H NMR (300 MHz, $CDCl_3$): δ = 8.86 (s, 8 H), 8.22 (m, 8 H), 7.77 (m, 11 H), 4.85 (s, 2 H), –2.78 (s, 2 H) ppm. ^{13}C NMR (75 MHz, $CDCl_3$): δ = 142.5, 142.2, 137.4, 135.1,

134.1, 131.2, 127.9, 127.6, 126.8, 120.5, 120.4, 119.3, 33.7 ppm. HRMS (MALDI-TOF): calcd. for $C_{45}H_{31}BrN_4$ 706.1732 $[M]^+$; found 706.1741.

Porphyrin 4: Porphyrin **3** (30 mg, 0.042 mmol), PPh_3 (33 mg, 0.126 mmol), and toluene (10 mL) were added into a round-bottomed flask. The mixture was heated at reflux for 3 h. Then, it was cooled to 0 °C for 1 h; this caused precipitation of the product, which was filtered and concentrated. The filtrate (5 mL) and PPh_3 (11 mg, 0.042 mmol) were added into a round-bottomed flask. The mixture was heated at reflux for another 3 h. Then, it was cooled to 0 °C for 1 h; this caused precipitation of the product, which was filtered. The precipitate was washed with toluene (25 mL) to obtain dark purple porphyrin **4**. Yield: 30 mg (74 %). ^{1}H NMR (500 MHz, $CDCl_3$): δ = 8.85 (m, 6 H), 8.71 (d, J = 5.0 Hz, 2 H), 8.20 (m, 6 H), 8.01 (m, 8 H), 7.86 (m, 3 H), 7.77 (m, 15 H), 7.52 (dd, J_1 = 8.0, J_2 = 2.5 Hz, 2 H), 5.91 (d, J = 14.0 Hz, 2 H), –2.82 (s, 2 H) ppm. ^{13}C NMR (75 MHz, $CDCl_3$): δ = 142.54, 142.48, 142.2, 135.31, 135.29, 135.01, 134.98, 134.8, 134.6, 131.5, 131.4, 131.3, 130.8, 130.6, 130.4, 130.0, 129.9, 127.9, 127.3, 127.2, 126.8, 120.6, 120.4, 118.8, 117.7, 31.3, 30.7 ppm. HRMS (MALDI-TOF): calcd. for $C_{63}H_{46}N_4P$ 889.3460 $[M - Br]^+$; found 889.3468.

5-{(*E*)-4-[4-({4-[(4-Formylphenyl)ethynyl]-2,5-bis[2-(2-methoxyethoxy)ethoxy]phenyl}ethynyl)styryl]phenyl}-10,15,20-triphenylporphyrin (6): Porphyrin **4** (30 mg, 0.031 mmol) and 4,4′-({2,5-bis[2-(2-methoxyethoxy)ethoxy]-1,4-phenylene}bis(ethyne-2,1-diyl))dibenzaldehyde (**5**; 21 mg, 0.037 mmol) were dissolved in dry CH_2Cl_2 (40 mL). LiOEt (1 M in EtOH, 375 µL, 0.116 mmol) was added dropwise, and the mixture was stirred at room temperature, protected from light. After 24 h, the reaction was quenched by the addition of dilute aqueous HCl (1 M). The organic layer was separated, washed with water, dried (Na_2SO_4), filtered, and concentrated. The product was purified by column chromatography (silica gel, CH_2Cl_2/EtOH, 98:2) to obtain purple porphyrin **6**. Yield: 12 mg (32 %). ^{1}H NMR (500 MHz, $CDCl_3$): δ = 10.03 (s, 1 H), 8.91 (d, J = 5 Hz, 2 H), 8.87 (m, 6 H), 8.23 (m, 8 H), 7.92 (d, J = 8 Hz, 2 H), 7.88 (d, J = 8 Hz, 2 H), 7.77 (m, 9 H), 7.69 (d, J = 8.5 Hz, 2 H), 7.67 (d, J = 8 Hz, 2 H), 7.61 (d, J = 8.5 Hz, 2 H), 7.49 (d, J = 16.5 Hz, 1 H), 7.42 (d, J = 16 Hz, 1 H), 7.12 (s, 1 H), 7.10 (s, 1 H), 4.27 (m, 4 H), 3.98 (m, 4 H), 3.87 (m, 2 H), 3.83 (m, 2 H), 3.59 (m, 4 H), 3.42 (s, 3 H), 3.39 (s, 3 H), –2.74 (s, 2 H) ppm. ^{13}C NMR (75 MHz, $CDCl_3$): δ = 191.6, 154.0, 153.7, 142.3, 142.0, 137.7, 136.5, 135.5, 135.3, 134.7, 132.2, 131.3, 129.7, 129.6, 128.8, 128.5, 127.9, 126.8, 125.1, 122.5, 120.4, 119.8, 117.6, 117.4, 117.3, 115.3, 113.4, 96.0, 94.3, 90.2, 86.9, 77.6, 77.2, 76.7, 72.2, 71.3, 71.2, 69.9, 69.8, 69.6, 59.2 ppm. HRMS (MALDI-TOF): calcd. for $C_{79}H_{65}N_4O_7$ 1181.4853 $[M + H]^+$; found 1181.4859.

(5-{(*E*)-4-[4-({4-[(4-Formylphenyl)ethynyl]-2,5-bis[2-(2-methoxyethoxy)ethoxy]phenyl}ethynyl)styryl]phenyl}-10,15,20-triphenylporphyrinato)zinc(II) (7): A solution of $Zn(CH_3COO)_2 \cdot 2H_2O$ (45 mg, 0.203 mmol) in CH_3OH (3 mL) was added to a solution of porphyrin **6** (24 mg, 0.020 mmol) in CH_2Cl_2 (15 mL), and the mixture was stirred at room temperature overnight. The crude residue was purified by column chromatography (silica gel, CH_2Cl_2/EtOH, 98:2) to obtain porphyrin **7** as a light-purple solid. Yield: 24 mg (96 %). ^{1}H NMR (500 MHz, $CDCl_3$): δ = 9.97 (s, 1 H), 9.01 (d, J = 4.5 Hz, 2 H), 8.95 (m, 6 H), 8.23 (m, 8 H), 7.91 (d, J = 8.0 Hz, 2 H), 7.82 (d, J = 8.0 Hz, 2 H), 7.77 (m, 9 H), 7.64 (d, J = 8.2 Hz, 2 H), 7.61 (d, J = 8.0 Hz, 2 H), 7.57 (d, J = 8.1 Hz, 2 H), 7.47 (d, J = 16.4 Hz, 1 H), 7.40 (d, J = 16.4 Hz, 1 H), 6.99 (s, 1 H), 6.98 (s, 1 H), 4.12 (m, 2 H), 4.00 (m, 2 H), 3.82 (m, 2 H), 3.67 (m, 4 H), 3.51 (m, 2 H), 3.40 (m, 2 H), 3.28 (m, 2 H), 3.26 (s, 3 H), 3.21 (s, 3 H) ppm. ^{13}C NMR (75 MHz, $CDCl_3$): δ = 191.6, 153.8, 153.5, 150.3, 150.2, 143.0, 142.8, 137.7, 136.2, 135.4, 135.1, 134.6, 132.1, 129.7, 128.6, 127.6, 126.7, 125.0, 122.4, 121.3, 120.7, 117.5, 117.2, 115.2, 113.2, 95.9, 94.2, 90.0, 86.8, 72.0, 71.9, 71.1, 70.8, 69.72, 69.67, 69.6, 69.4, 59.11, 59.06 ppm. HRMS (MALDI-TOF): calcd. for $C_{79}H_{62}N_4O_7Zn$ 1242.3910 $[M]^+$; found 1242.3918.

{5-[4-((*E*)-4-{[4-({4-[(*Z*)-2-Carboxy-2-cyanovinyl]phenyl}ethynyl)-2,5-bis[2-(2-methoxyethoxy)ethoxy]phenyl]ethynyl}styryl)-phenyl]-10,15,20-triphenylporphyrinato}zinc(II) [ZnP(SP)-CNCOOH]: 2-Cyanocetic acid (9 mg, 0.102 mmol) and piperidine (5 µL) were added to a solution of **7** (21 mg, 0.017 mmol) in THF (2 mL), and the mixture was heated to 65 °C under N_2 for 24 h. The solvents were evaporated under reduced pressure. The solid was dissolved in CH_2Cl_2 (10 mL) and washed with 0.5 M H_3PO_4 (2 × 20 mL). CH_2Cl_2 was removed under vacuum, and the product was purified by column chromatography (silica gel, CH_2Cl_2/MeOH, 9:1) to obtain dark red-purple porphyrin ZnP(SP)CNCOOH. Yield: 10 mg (43 %). ^{1}H NMR (500 MHz, DMSO): δ = 8.86 (d, J = 4.6 Hz, 2 H), 8.78 (m, 6 H), 8.20 (m, 8 H), 8.14 (s, 1 H), 8.04 (m, 4 H), 7.82 (m, 11 H), 7.72 (d, J = 16.3 Hz, 1 H), 7.68 (d, J = 8.2 Hz, 2 H), 7.64 (m, 3 H), 7.28 (s, 2 H), 4.23 (m, 4 H), 3.84 (m, 4 H), 3.72 (m, 4 H), 3.49 (m, 4 H), 3.28 (s, 3 H), 3.24 (s, 3 H) ppm. Due to solubility reasons, we were unable to record a ^{13}C NMR spectrum for ZnP(SP)CNCOOH. UV/Vis (CH_2Cl_2): λ_{max} (ε, mM^{-1} cm^{-1}) = 422 (275.0), 548 (13.1), 587 nm (3.7). HRMS (MALDI-TOF): calcd. for $C_{82}H_{63}N_5O_8Zn$ 1309.3968 $[M]^+$; found 1309.3961.

[5-(4-Formylphenyl)-10,15,20-triphenylporphyrinato]zinc(II) (9): A solution of $Zn(CH_3COO)_2 \cdot 2H_2O$ (163 mg, 0.745 mmol) in CH_3OH (10 mL) was added to a solution of porphyrin **8** (48 mg, 0.0745 mmol) in CH_2Cl_2 (50 mL), and the mixture was stirred at room temperature overnight. The crude residue was purified by column chromatography (silica gel, CH_2Cl_2) to obtain porphyrin **8** as a red-purple solid. Yield: 52 mg (98 %). ^{1}H NMR (500 MHz, $CDCl_3$): δ = 10.34 (s, 1 H), 8.98 (d, J = 5.0 Hz, 2 H), 8.96 (s, 4 H), 8.88 (d, J = 4.5 Hz, 2 H), 8.41 (d, J = 8.0 Hz, 2 H), 8.27 (d, J = 8.0 Hz, 2 H), 8.22 (m, 6 H), 7.77 (m, 9 H) ppm. ^{13}C NMR (75 MHz, $CDCl_3$): δ = 192.7, 150.6, 150.5, 150.3, 149.6, 149.5, 142.8, 135.5, 135.2, 134.6, 132.6, 132.4, 132.3, 131.5, 128.1, 127.7, 126.7, 121.8, 121.6, 119.2 ppm. HRMS (MALDI-TOF): calcd. for $C_{45}H_{28}N_4OZn$ 704.1555 $[M]^+$; found 704.1562.

{5-[(*Z*)-4-(2-Carboxy-2-cyanovinyl)phenyl]-10,15,20-triphenylporphyrinato}zinc(II) (ZnPCNCOOH): 2-Cyanoacetic acid (15 mg, 0.18 mmol) and piperidine (9 µL) were added to a solution of porphyrin **9** (25 mg, 0.03 mmol) in THF (4 mL), and the mixture was heated to 65 °C under a N_2 atmosphere overnight. The solvents were evaporated under reduced pressure, and the product was purified by column chromatography (silica gel, CH_2Cl_2/EtOH, 97:3) to obtain porphyrin ZnPCNCOOH as a green-purple solid. Yield: 15 mg (56 %). ^{1}H NMR (500 MHz, DMSO): δ = 8.82 (d, J = 4.5 Hz, 2 H), 8.79 (d, J = 4.5 Hz, 2 H), 8.78 (m, 4 H), 8.53 (s, 1 H), 8.41 (d, J = 8.0 Hz, 2 H), 8.36 (d, J = 8.0 Hz, 2 H), 8.19 (m, 6 H), 7.83 (m, 9 H) ppm. ^{13}C NMR (75 MHz, DMSO): δ = 163.2, 157.9, 149.5, 149.3, 148.9, 146.7, 142.7, 135.0, 134.2, 132.0, 131.7, 131.5, 128.5, 127.6, 126.7, 120.8, 120.6, 119.0, 117.8 ppm. UV/Vis (DMSO): λ_{max} (ε, mM^{-1} cm^{-1}) = 428 (230.0), 561 (11.0), 601 nm (5.5). HRMS (MALDI-TOF): calcd. for $C_{48}H_{29}N_5O_2Zn$ 771.1613 $[M]^+$; found 771.1619.

Supporting Information (see footnote on the first page of this article): Tables with X-ray crystallographic information for **4**·1.5H_2O, additional photophysics measurements and spectroscopic data, coordinates of the gas-phase-optimized structures of ZnPCNCOOH and ZnP(SP)CNCOOH, as calculated by DFT.

Acknowledgments

This work was supported by the European Commission's Seventh Framework Programme (FP7/2007-2013) under grant agreement no. 229927 (FP7-REGPOT-2008-1, Project BIOSOLENUTI). The Special Research Account of the University of Crete is also acknowledged.

Keywords: Photovoltaics · Porphyrins · Sensitizers · Solar cells · Zinc

[1] a) M. Janani, P. Srikrishnarka, S. V. Nair, A. S. Nair, *J. Mater. Chem. A* **2015**, *3*, 17914–17938; b) K. J. Young, L. A. Martini, R. L. Milot, R. C. Snoeberger, V. S. Batista, C. A. Schmuttenmaer, R. H. Crabtree, G. W. Brudvig, *Coord. Chem. Rev.* **2012**, *256*, 2503–2520; c) V. Nikolaou, A. Charisiadis, G. Charalambidis, A. G. Coutsolelos, F. Odobel, *J. Mater. Chem. A* **2017**, *5*, 21077–21113; d) N. Sharifi, F. Tajabadi, N. Taghavinia, *ChemPhysChem* **2014**, *15*, 3902–3927.

[2] B. O'Regan, M. Grätzel, *Nature* **1991**, *353*, 737–740.

[3] a) L.-L. Li, E. W.-G. Diau, *Chem. Soc. Rev.* **2013**, *42*, 291–304; b) K. Ladomenou, V. Nikolaou, G. Charalambidis, A. G. Coutsolelos, *Dalton Trans.* **2016**, *45*, 1111–1126; c) Ö. Birel, S. Nadeem, H. Duman, *J. Fluoresc.* **2017**, *27*, 1075–1085.

[4] a) C. Stangel, C. Schubert, S. Kuhri, G. Rotas, J. T. Margraf, E. Regulska, T. Clark, T. Torres, N. Tagmatarchis, A. G. Coutsolelos, D. M. Guldi, *Nanoscale* **2015**, *7*, 2597–2608; b) C. B. Kc, F. D'Souza, *Coord. Chem. Rev.* **2016**, *322*, 104–141; c) A. Bagaki, H. B. Gobeze, G. Charalambidis, A. Charisiadis, C. Stangel, V. Nikolaou, A. Stergiou, N. Tagmatarchis, F. D'Souza, A. G. Coutsolelos, *Inorg. Chem.* **2017**, *56*, 10268–10280; d) K. Ladomenou, V. Nikolaou, G. Charalambidis, A. Charisiadis, A. G. Coutsolelos, *C. R. Chim.* **2017**, *20*, 314–322; e) C. Stangel, A. Charisiadis, G. E. Zervaki, V. Nikolaou, G. Charalambidis, A. Kahnt, G. Rotas, N. Tagmatarchis, A. G. Coutsolelos, *J. Phys. Chem. C* **2017**, *121*, 4850–4858.

[5] a) K. T. Weber, K. Karikis, M. D. Weber, P. B. Coto, A. Charisiadis, D. Charitaki, G. Charalambidis, P. Angaridis, A. G. Coutsolelos, R. D. Costa, *Dalton Trans.* **2016**, *45*, 13284–13288; b) A. Coutsolelos, R. Guilard, A. Boukhris, C. Lecomte, *J. Chem. Soc., Dalton Trans.* **1986**, 1779–1783; c) E. M. Davoras, G. A. Spyroulias, E. Mikros, A. G. Coutsolelos, *Inorg. Chem.* **1994**, *33*, 3430–3434; d) K. M. Kadish, J. L. Cornillon, A. Coutsolelos, R. Guilard, *Inorg. Chem.* **1987**, *26*, 4167–4173; e) G. D. Sharma, G. E. Zervaki, P. A. Angaridis, T. N. Kitsopoulos, A. G. Coutsolelos, *J. Phys. Chem. C* **2014**, *118*, 5968–5977; f) M. J. Tornaritis, A. G. Coutsolelos, *Polymer* **1992**, *33*, 1771–1772.

[6] M. Urbani, M. Grätzel, M. K. Nazeeruddin, T. Torres, *Chem. Rev.* **2014**, *114*, 12330–12396.

[7] a) T. Higashino, H. Imahori, *Dalton Trans.* **2015**, *44*, 448–463; b) H. Song, X. Li, H. Ågren, Y. Xie, *Dyes Pigm.* **2017**, *137*, 421–429; c) T. Higashino, K. Kawamoto, K. Sugiura, Y. Fujimori, Y. Tsuji, K. Kurotobi, S. Ito, H. Imahori, *ACS Appl. Mater. Interfaces* **2016**, *8*, 15379–15390; d) A. Yella, H.-W. Lee, H. N. Tsao, C. Yi, A. K. Chandiran, M. K. Nazeeruddin, E. W.-G. Diau, C.-Y. Yeh, S. M. Zakeeruddin, M. Grätzel, *Science* **2011**, *334*, 629–634.

[8] a) S. Mathew, A. Yella, P. Gao, R. Humphry-Baker, B. F. E. Curchod, N. Ashari-Astani, I. Tavernelli, U. Rothlisberger, M. K. Nazeeruddin, M. Grätzel, *Nat. Chem.* **2014**, *6*, 242; b) A. Yella, C.-L. Mai, S. M. Zakeeruddin, S.-N. Chang, C.-H. Hsieh, C.-Y. Yeh, M. Grätzel, *Angew. Chem. Int. Ed.* **2014**, *53*, 2973–2977; *Angew. Chem.* **2014**, *126*, 3017–3021.

[9] a) M. Ishida, D. Hwang, Y. B. Koo, J. Sung, D. Y. Kim, J. L. Sessler, D. Kim, *Chem. Commun.* **2013**, *49*, 9164–9166; b) G. Di Carlo, A. Orbelli Biroli, F. Tessore, M. Pizzotti, P. R. Mussini, A. Amat, F. De Angelis, A. Abbotto, V. Trifiletti, R. Ruffo, *J. Phys. Chem. C* **2014**, *118*, 7307–7320; c) F. Lu, Y. Feng, X. Wang, Y. Zhao, G. Yang, J. Zhang, B. Zhang, Z. Zhao, *Dyes Pigm.* **2017**, *139*, 255–263; d) G. Di Carlo, A. O. Biroli, F. Tessore, S. Caramori, M. Pizzotti, *Coord. Chem. Rev.* **2018**, *358*, 153–177.

[10] a) J. S. Lindsey, *Acc. Chem. Res.* **2010**, *43*, 300–311; b) A. Orbelli Biroli, F. Tessore, V. Vece, G. Di Carlo, P. R. Mussini, V. Trifiletti, L. De Marco, R. Giannuzzi, M. Manca, M. Pizzotti, *J. Mater. Chem. A* **2015**, *3*, 2954–2959.

[11] a) A. Hagfeldt, G. Boschloo, L. Sun, L. Kloo, H. Pettersson, *Chem. Rev.* **2010**, *110*, 6595–6663; b) K. Ladomenou, T. N. Kitsopoulos, G. D. Sharma, A. G. Coutsolelos, *RSC Adv.* **2014**, *4*, 21379–21404; c) A. Charisiadis, C. Stangel, V. Nikolaou, M. S. Roy, G. D. Sharma, A. G. Coutsolelos, *RSC Adv.* **2015**, *5*, 88508–88519; d) Q. Zhang, J. Sun, K.-X. Shang, J.-C. Liu, R.-Z. Li, N.-Z. Jin, *J. Coord. Chem.* **2017**, *70*, 780–789; e) V. Nikolaou, A. Charisiadis, S. Chalkiadaki, I. Alexandropoulos, S. C. Pradhan, S. Soman, M. K. Panda, A. G. Coutsolelos, *Polyhedron* **2018**, *140*, 9–18.

[12] a) E. M. Barea, R. Caballero, L. López-Arroyo, A. Guerrero, P. de la Cruz, F. Langa, J. Bisquert, *ChemPhysChem* **2011**, *12*, 961–965; b) F. Lu, Q. Zeng, H. Duan, *ACM Trans. Knowl. Discov. Data* **2016**, *10*, 1–29; c) J. Luo, J. Zhang, K.-W. Huang, Q. Qi, S. Dong, J. Zhang, P. Wang, J. Wu, *J. Mater. Chem. A* **2016**, *4*, 8428–8434.

[13] a) C. Stangel, A. Bagaki, P. A. Angaridis, G. Charalambidis, G. D. Sharma, A. G. Coutsolelos, *Inorg. Chem.* **2014**, *53*, 11871–11881; b) L. Han, A. Islam, H. Chen, C. Malapaka, B. Chiranjeevi, S. Zhang, X. Yang, M. Yanagida, *Energy Environ. Sci.* **2012**, *5*, 6057–6060.

[14] P. Demay-Drouhard, H. Y. V. Ching, D. Akhmetzyanov, R. Guillot, L. C. Tabares, H. C. Bertrand, C. Policar, *ChemPhysChem* **2016**, *17*, 2066–2078.

[15] G. Q. Liu, A. N. Khlobystov, G. Charalambidis, A. G. Coutsolelos, G. A. D. Briggs, K. Porfyrakis, *J. Am. Chem. Soc.* **2012**, *134*, 1938–1941.

[16] a) A. Charisiadis, V. Nikolaou, K. Karikis, C. Giatagana, K. Chalepli, K. Ladomenou, S. Biswas, G. D. Sharma, A. G. Coutsolelos, *New J. Chem.* **2016**, *40*, 5930–5941; b) J. A. Mikroyannidis, G. Charalambidis, A. G. Coutsolelos, P. Balraju, G. D. Sharma, *J. Power Sources* **2011**, *196*, 6622–6628; c) G. D. Sharma, D. Daphnomili, S. Biswas, A. G. Coutsolelos, *Org. Electron.* **2013**, *14*, 1811–1819; d) G. E. Zervaki, E. Papastamatakis, P. A. Angaridis, V. Nikolaou, M. Singh, R. Kurchania, T. N. Kitsopoulos, G. D. Sharma, A. G. Coutsolelos, *Eur. J. Inorg. Chem.* **2014**, 1020–1033.

[17] Y. Liang, X. Xue, W. Zhang, C. Fan, Y. Li, B. Zhang, Y. Feng, *Dyes Pigm.* **2015**, *115*, 7–16.

[18] A. S. Shalabi, A. M. El Mahdy, M. M. Assem, H. O. Taha, K. A. Soliman, *J. Nanopart. Res.* **2014**, *16*, 2579.

[19] Y. Wang, B. Chen, W. Wu, X. Li, W. Zhu, H. Tian, Y. Xie, *Angew. Chem. Int. Ed.* **2014**, *53*, 10779–10783; *Angew. Chem.* **2014**, *126*, 10955–10959.

[20] S. Ahmad, E. Guillén, L. Kavan, M. Grätzel, M. K. Nazeeruddin, *Energy Environ. Sci.* **2013**, *6*, 3439–3466.

[21] C. Li, L. Luo, D. Wu, R. Jiang, J. Lan, R. Wang, L. Huang, S. Yang, J. You, *J. Mater. Chem. A* **2016**, *4*, 11829–11834.

[22] a) J. Bisquert, *Phys. Chem. Chem. Phys.* **2003**, *5*, 5360–5364; b) D. Kuang, S. Uchida, R. Humphry-Baker, S. M. Zakeeruddin, M. Grätzel, *Angew. Chem. Int. Ed.* **2008**, *47*, 1923–1927; *Angew. Chem.* **2008**, *120*, 1949–1953.

[23] T. Zhang, X. Qian, P.-F. Zhang, Y.-Z. Zhu, J.-Y. Zheng, *Chem. Commun.* **2015**, *51*, 3782–3785.

[24] S. Chang, H. Wang, Y. Hua, Q. Li, X. Xiao, W.-K. Wong, W. Y. Wong, X. Zhu, T. Chen, *J. Mater. Chem. A* **2013**, *1*, 11553–11558.

[25] Z.-S. Huang, X.-F. Zang, T. Hua, L. Wang, H. Meier, D. Cao, *ACS Appl. Mater. Interfaces* **2015**, *7*, 20418–20429.

[26] a) L. Bertoluzzi, S. Ma, *Phys. Chem. Chem. Phys.* **2013**, *15*, 4283–4285; b) P.-T. Hsiao, Y.-L. Tung, H. Teng, *J. Phys. Chem. C* **2010**, *114*, 6762–6769.

[27] *Program for the Acquisition and Analysis Data* (version 1.30), Stoe & Cie GmbH, Darmstadt, Germany, **2005**.

[28] Program for Data Reduction and Absorption Correction (version 1.28b), Stoe & Cie GmbH, Darmstadt, Germany, **2005**.

[29] *Program for Crystal Optimization for Numerical Absorption Correction* (version 2.05), Stoe & Cie GmbH, Darmstadt, Germany, **2004**.

[30] a) C. B. Hübschle, G. M. Sheldrick, B. Dittrich, *J. Appl. Crystallogr.* **2011**, *44*, 1281–1284; b) G. M. Sheldrick, *Acta Crystallogr., Sect. A* **2008**, *64*, 112–122.

[31] G. M. Sheldrick, *Program for Crystal Structure Refinement* (version 2014/7), University of Göttingen, **2014**.

[32] a) A. L. Spek, *J. Appl. Crystallogr.* **2003**, *36*, 7–13; b) A. L. Spek, *Acta Crystallogr., Sect. D* **2009**, *65*, 148–155; c) A. L. Spek, *Acta Crystallogr., Sect. C* **2015**, *71*, 9–18.

[33] W. Kohn, L. J. Sham, *Phys. Rev.* **1965**, *140*, A1133–A1138.

[34] a) A. D. Becke, *Phys. Rev. A* **1988**, *38*, 3098–3100; b) C. Lee, W. Yang, R. G. Parr, *Phys. Rev. B* **1988**, *37*, 785–789.

[35] M. J. Frisch, H. B. Schlegel, G. E. Scuseria, M. A. Robb, J. R. Cheeseman, J. A. Montgomery Jr., T. Vreven, K. N. Kudin, J. C. Burant, J. M. Millam, S. S. Lyengar, J. Tomasi, V. Barone, B. Mennucci, M. Cossi, G. Scalmani, N. Rega, G. A. Petersson, H. Nakatsuji, M. Hada, M. Ehara, K. Toyota, R. Fukuda, J. Hasegawa, M. Ishida, T. Nakajima, Y. Honda, O. Kitao, H. Nakai,

M. Klene, X. Li, J. E. Knox, H. P. Hratchian, J. B. Cross, V. Bakken, C. Adamo, J. Jaramillo, R. Gomperts, R. E. Stratmann, O. Yazyev, A. J. Austin, R. Cammi, C. Pomelli, J. W. Ochterski, P. Y. Ayala, K. Morokuma, G. A. Voth, P. Salvador, J. J. Dannenberg, V. G. Zakrzewski, S. Dapprich, A. D. Daniels, M. C. Strain, O. Farkas, D. K. Malick, A. D. Rabuck, K. Raghavachari, J. B. Foresman, J. V. Ortiz, Q. Cui, A. G. Baboul, S. Clifford, J. Cioslowski, B. B. Stefanov, G. Liu, A. Liashenko, P. Piskorz, I. Komaromi, R. L. Martin, D. J. Fox, T. Keith, M. A. Al-Laham, C. Y. Peng, A. Nanayakkara, M. Challacombe, P. M. W. Gill, B. Johnson, W. Chen, M. W. Wong, C. Gonzalez, J. A. Pople, *Gaussian 03*, *Revision D.01*, Gaussian, Inc., Wallingford, CT, **2004**.

[36] M. Cossi, V. Barone, R. Cammi, J. Tomasi, *Chem. Phys. Lett.* **1996**, *255*, 327–335.

[37] D. A. Zhurko, G. A. Zhurko, *ChemCraft 1.6*, Plimus, San Diego, CA. Available at http://www.chemcraftprog.com.

Received: January 29, 2018